

## Zeeman spectroscopy as a method for determining the magnetic field distribution in self-magnetic-pinch diodes (invited)

S. G. Patel, M. D. Johnston, T. J. Webb, N. L. Bennett, D. R. Welch, R. M. Gilgenbach, M. E. Cuneo, M. L. Kiefer, J. J. Leckbee, M. G. Mazarakis, D. J. Muron, T. J. Renk, S. C. Simpson, R. Doron, S. Biswas, D. Mikitchuk, and Y. Maron

Citation: [Review of Scientific Instruments](#) **89**, 10D123 (2018); doi: 10.1063/1.5039386

View online: <https://doi.org/10.1063/1.5039386>

View Table of Contents: <http://aip.scitation.org/toc/rsi/89/10>

Published by the [American Institute of Physics](#)

---

### Articles you may be interested in

[Development of a high current 60 keV neutral lithium beam injector for beam emission spectroscopy measurements on fusion experiments](#)

[Review of Scientific Instruments](#) **89**, 013503 (2018); 10.1063/1.5004126

[Effects of stray lights on Faraday rotation measurement for polarimeter-interferometer system on EAST](#)

[Review of Scientific Instruments](#) **89**, 013510 (2018); 10.1063/1.5012820

[Ultrafast two-dimensional lithium beam emission spectroscopy diagnostic on the EAST tokamak](#)

[Review of Scientific Instruments](#) **89**, 063503 (2018); 10.1063/1.5017224

[Influence of neutral beam attenuation on beam emission spectroscopy and charge exchange recombination spectroscopy](#)

[Review of Scientific Instruments](#) **89**, 073503 (2018); 10.1063/1.5028205

[Simultaneous measurement of C VI, Ne X, and Li III charge exchange lines on EAST](#)

[Review of Scientific Instruments](#) **89**, 10D119 (2018); 10.1063/1.5036835

[Zeeman splitting measurements of magnetic fields in iodine plasma](#)

[Review of Scientific Instruments](#) **89**, 10C113 (2018); 10.1063/1.5038641

---



**PFEIFFER VACUUM**

**VACUUM SOLUTIONS FROM A SINGLE SOURCE**

Pfeiffer Vacuum stands for innovative and custom vacuum solutions worldwide, technological perfection, competent advice and reliable service.

[Learn more!](#)

# Zeeman spectroscopy as a method for determining the magnetic field distribution in self-magnetic-pinch diodes (invited)

S. G. Patel,<sup>1,a)</sup> M. D. Johnston,<sup>1</sup> T. J. Webb,<sup>1</sup> N. L. Bennett,<sup>1</sup> D. R. Welch,<sup>1</sup> R. M. Gilgenbach,<sup>2</sup> M. E. Cuneo,<sup>1</sup> M. L. Kiefer,<sup>1</sup> J. J. Leckbee,<sup>1</sup> M. G. Mazarakis,<sup>1</sup> D. J. Muron,<sup>1</sup> T. J. Renk,<sup>1</sup> S. C. Simpson,<sup>1</sup> R. Doron,<sup>3</sup> S. Biswas,<sup>3</sup> D. Mikitchuk,<sup>3</sup> and Y. Maron<sup>3</sup>

<sup>1</sup>Sandia National Laboratories, Albuquerque, New Mexico 87185, USA

<sup>2</sup>University of Michigan, Ann Arbor, Michigan 48109, USA

<sup>3</sup>Weizmann Institute of Science, Rehovot 76100, Israel

(Presented 18 April 2017; received 7 May 2018; accepted 25 June 2018; published online 8 October 2018)

In the self-magnetic-pinch diode, the electron beam, produced through explosive field emission, focuses on the anode surface due to its own magnetic field. This process results in dense plasma formation on the anode surface, consisting primarily of hydrocarbons. Direct measurements of the beam's current profile are necessary in order to understand the pinch dynamics and to determine x-ray source sizes, which should be minimized in radiographic applications. In this paper, the analysis of the C IV doublet (580.1 and 581.2 nm) line shapes will be discussed. The technique yields estimates of the electron density and electron temperature profiles, and the method can be highly beneficial in providing the current density distribution in such diodes. *Published by AIP Publishing.* <https://doi.org/10.1063/1.5039386>

## I. INTRODUCTION

The Self-Magnetic-Pinch (SMP) diode<sup>1</sup> was designed as an electron beam source for use in flash x-ray radiography. The beam is produced through explosive field emission, as the cathode surface breaks down and plasma formation occurs.<sup>2</sup> The planar anode consists of a high-Z target material, such as tantalum, which converts the beam energy into bremsstrahlung x-rays. The electron beam impacts the anode and heats the anode surface to temperatures greater than 400 °C within a few nanoseconds, desorbing contaminants<sup>3</sup> and forming a dense surface plasma, which is shown in Fig. 1.

In the standard SMP diode configuration, a thin Al-foil is placed about 1 mm from the anode surface. This foil is transparent to the electron beam and extends the x-ray pulse, which is ideally around 60 ns, by delaying plasma expansion into the anode-cathode (AK) gap.<sup>4</sup> As the electrode plasma expands into the AK gap, its charge partially neutralizes the beam charge.<sup>5</sup> Consequently, measurements of the beam's self-magnetic field are critical to understanding the pinch dynamics throughout the current pulse and predicting x-ray source sizes, which should be minimized to reduce the image blur for radiography.

Time-resolved spot size measurements show minimum x-ray source diameters to be less than 3 mm,<sup>1</sup> with current densities of around 10 MA/cm<sup>2</sup>.<sup>6</sup> Beam current measurements are also performed using *B*-dot probes placed behind the cathode, as shown in Fig. 2. These probes measure the bipolar current, which includes the electron beam current and the

back-streaming ion current, determined to be about 10%-30% of the total current.<sup>7</sup> However, these measurements are limited to outside the AK gap and therefore cannot be used to determine the current distribution within the diode. In this paper, we investigate the Zeeman splitting of spectral lines as a method for measuring the magnetic field distribution in the diode.

### A. Zeeman splitting

The electron beam produces an azimuthal magnetic field, assuming cylindrical symmetry of the beam. Measurements of the current profiles are performed using the weak field approximation of the Zeeman effect on emission lines. In this approximation of the Zeeman effect, when an external magnetic field is applied, the atomic fine structure splits into  $2J + 1$  (where *J* is the angular momentum of the level) energy levels, and the magnetic field is proportional to the energy shift of the atomic level. The energy shift of each level is given by

$$\Delta E = \mu_B g m_j B, \quad (1)$$

where  $\mu_B$  is the Bohr magneton, *g* is the Lande *g*-factor, *B* is the applied magnetic field, and  $m_j$  is the projection of *J* along the direction of the applied magnetic field. The Zeeman pattern consists of both  $\pi$  ( $\Delta m_j = 0$ ) and  $\sigma$  polarizations ( $\Delta m_j = \pm 1$ ), and the intensities of the individual Zeeman components are given in Ref. 8.

## II. EXPERIMENTAL CONFIGURATION

The experimental configuration consisted of eleven, 200  $\mu\text{m}$  fibers arranged in a single row, as shown in Fig. 2. The array imaged along 1 mm diameter chords across the anode

Note: Paper published as part of the Proceedings of the 22nd Topical Conference on High-Temperature Plasma Diagnostics, San Diego, California, April 2018.

<sup>a)</sup> Author to whom correspondence should be addressed: spatel@sandia.gov.

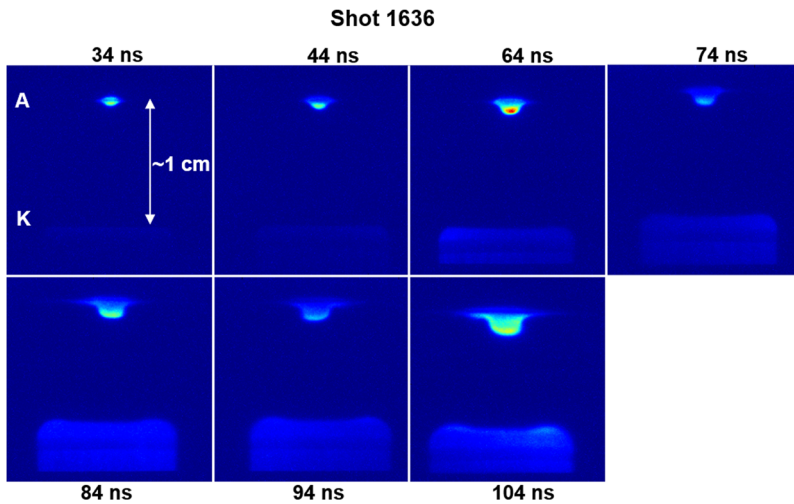


FIG. 1. A multi-frame camera imaged the electrode plasma expansion into the gap, with the first image approximately 34 ns after the start of current, see Fig. 6. The central plume on the anode was used to determine radial plasma expansion velocities to establish the effect of Doppler shifts on the measured spectrum. A and K represent the anode and cathode location, respectively.

surface during the current pulse. A schematic of this chordal line of sight is shown in Fig. 3. The fiber array was lens coupled to a 0.32 m Princeton Instruments IsoPlane SCT-320 spectrometer. The design of this spectrometer reduces some of the image

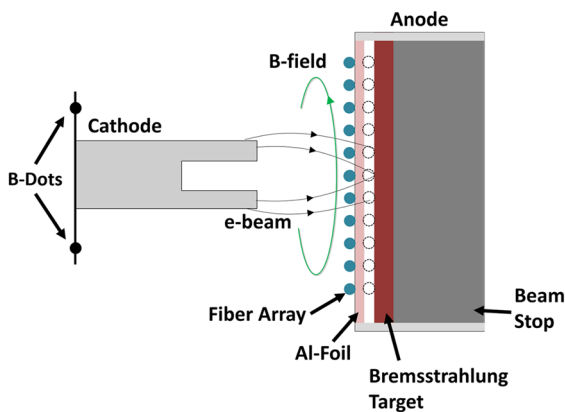


FIG. 2. Four B-dots are placed 90° apart behind the cathode to measure the beam current and the current due to back streaming ions from the anode surface plasma. The 11-fiber array images the foil surface (filled circles) or the anode target (unfilled circles), depending on the diode configuration.

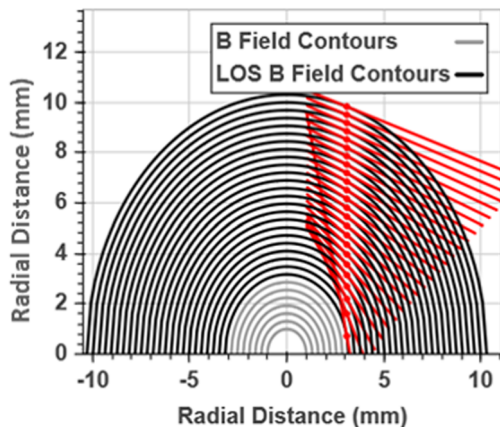


FIG. 3. A simplified diagram of the chordal line of sight at about 3 mm across the anode surface. Magnetic field contours are plotted in black, for those along the chordal view, and in gray for contours not along the line of sight.

aberrations that occur in a standard Czerny-Turner system, such as spherical aberrations, coma effects, and astigmatism, which is particularly important when imaging off-axis, multi-fiber inputs, such as those described in this paper. A Princeton Instruments PI-Max camera was placed at the focal plane of the spectrometer. The single frame camera was gated for 10-15 ns during the x-ray pulse of the SMP diode. In this configuration, the spectrometer with a 2400 g/mm grating, and 50 μm slit, resulted in a spectral resolution of 0.065 nm, measured using the width of Hg I lines from a mercury pen lamp.

The probe is calibrated for relative intensity by using a tungsten light source, with a known spectral radiance, coupled through an integrating sphere. Multiple reflections within the sphere result in a uniform light source at the output. Preferably, this calibration would use the same gate time as used on a typical shot. However, for these experiments the intensified charge-coupled device (ICCD) was gated for 10-15 ns, which is too short to obtain enough signal from the blackbody calibration source. Therefore, the lamp was gated for about 5 ms to obtain a relative intensity calibration.

The current profiles are determined from C IV 5801.3 and 5812.0 Å doublet lines. Carbon is primarily a contaminant in the vacuum chamber and is not localized on the anode surface. As a result, localized measurements must be inferred from the chordal line of sight in order to determine the current profile in the diode.

### III. ANALYSIS

The 200-μm fibers coupled with a 150-mm focal length lens result in a depth of field of about 3.4 cm. In practice, there is very little light outside the extent of the fiber array, and consequently the fitting algorithm discretizes a 2 cm chordal line of sight into 200 points and calculates the magnetic field and the angle of the field to the line of sight at each point, as shown in Fig. 3. The Zeeman components are estimated to be a Voigt profile with Stark broadening forming the Lorentzian part. Thermal Doppler and instrument broadening compose the Gaussian portion. Opacity effects are assumed to be negligible as the ratio of the relative intensities of the C IV doublet (1/2-1/2 transition to the 3/2-1/2 transition) is 0.5.

Each discretized point also has varying contributions to the total spectrum since the C IV line intensity drops with distance from the beam axis. To account for this, the radial intensity profile of the C IV doublet is obtained by performing an Abel inversion of the line-integrated profiles, and each of the 200 discretized points is weighted by the estimated normalized intensity. An example of the radial C IV normalized relative intensity distribution is shown in Fig. 4 for Shot 1919. A Gaussian profile was used to approximate this distribution, after subtracting the background. The C IV line is seen to peak at about 6 mm.

The sum of the discretized calculated spectra is then fit to the data with a Levenberg-Marquardt curve fitting algorithm.<sup>9</sup> A simplified diagram of this process is shown in Fig. 3. Additionally, the radial location of each fiber must be known precisely in order to determine the current density within the diode. This is determined post-shot to account for alignment uncertainties and beam motion. The average of the continuum intensity of each of the eleven fibers is fit with a Gaussian profile. The peak of the profile is then taken to be the beam axis.

Spectroscopic measurements during the pulse showed strong hydrogen and carbon line emission. Line splitting is measured on the C IV 4s-4p transition, as shown in Fig. 5, particularly at radii greater than about 5 mm. At smaller radii, where the electron densities are higher and the line shape is dominated by Stark broadening, the 1/2-1/2 transition is slightly broader than the 3/2-1/2 transition, which is a clear indication of a magnetic field since all other broadening mechanisms, such as Stark and Doppler effects, are the same for both lines.<sup>10</sup> For example, in Fig. 5(a), the full width at half maximum of the 1/2-1/2 transition is about 15% larger when compared to the 3/2-1/2 transition and is accurately fit by including a magnetic field.

The ratio of the relative intensity of C IV to C III emission lines was used to estimate the electron temperature. These ratios were compared to a PrismSPECT<sup>11</sup> non-LTE, optically

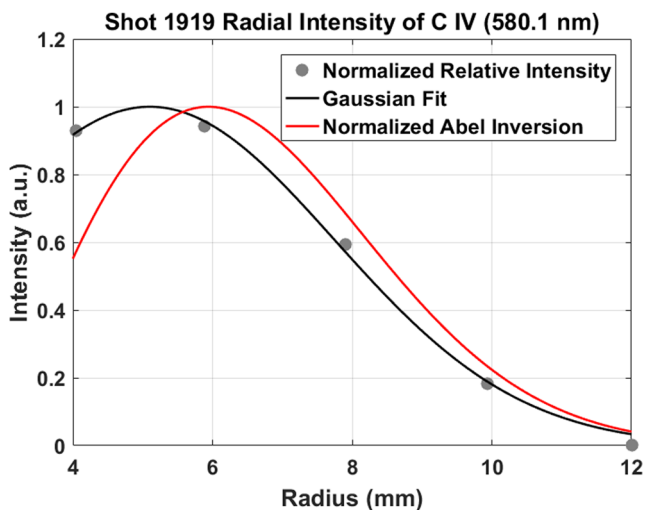


FIG. 4. The radial relative intensity distribution for the C IV line at 580.133 nm. The relative intensity is fit with a Gaussian profile (black), and an Abel inversion (red) is performed on this profile to obtain intensity as a function of radius.

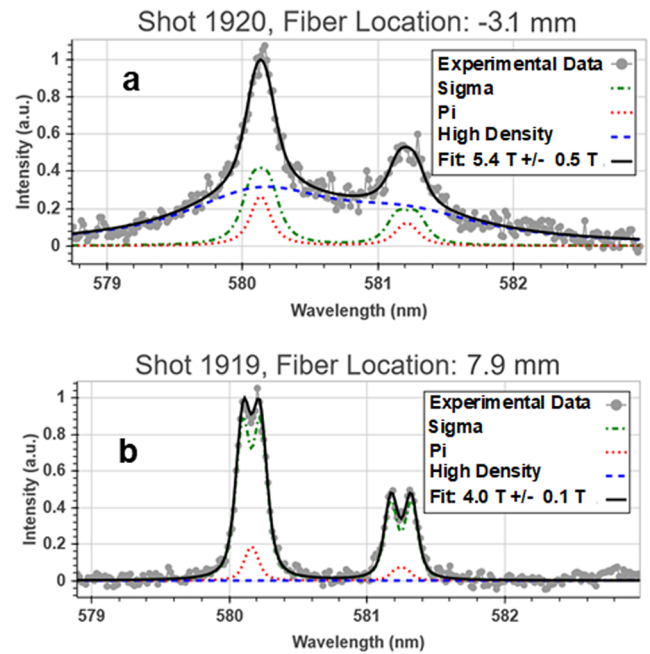


FIG. 5. Two example fits of the Zeeman split C IV doublet, resulting in an upper bound on the magnetic field at these locations. Both  $\pi$  (red) and  $\sigma$  (green) components are visible due to the curved magnetic field. Fitting errors are estimated in these figures. (a) This spectrum was taken at about 3 mm from the axis. A two density region is assumed for spectra close to the beam axis due to large density gradients along the line of sight at these locations, due to a dense surface plasma. The dashed blue line represents a higher density but lower intensity component in order to accurately fit the wide wings. (b) This spectrum was taken at a radius of about 7.9 mm. Farther from the axis, a single density approximation can accurately reflect the spectrum since there are fewer variations along the chord.

thin, quasistatic model for a pure carbon plasma. This suggested electron temperatures between 5.5 and 6.5 eV.<sup>11</sup> As a result, thermal Doppler broadening adds roughly 0.06 nm to the Gaussian width, assuming the electron and ion densities are equal. However, ion temperatures ranging from 2 to 7 eV result in only a 5% uncertainty in the electron densities with the B-field estimates remaining essentially the same. Radial expansion velocities, measured from several multi-frame camera images—for example, shown in Fig. 1—are estimated to be about 1.37 cm/ $\mu$ s. Doppler shifts as a result of these velocities along the line of sight are essentially negligible in comparison to Stark broadening and do not contribute noticeably to the line splitting. Due to the chordal line of sight, expansion velocities would have to be about 8-10 cm/ $\mu$ s for the outer chords and 3-4 cm/ $\mu$ s for the inner chords. Although the velocities are calculated from images which only show plasma formation within a few millimeters of the axis, and not the outer regions where Zeeman splitting is observed, it is unlikely that the lower pressure regions further from the axis would expand faster than the central regions, especially since the electric field is axial.

B-dot traces are plotted in Fig. 6 for several shots. The traces show currents within the spectrometer gate to range between 120 and 150 kA. Shots 1959 and 1960 were on a standard SMP diode configuration which consisted of an aluminum foil placed about 1 mm from a tantalum bremsstrahlung target. Shots 1919 and 1920 were taken on a carbon-coated tantalum target and a silicon-coated tungsten target, respectively.

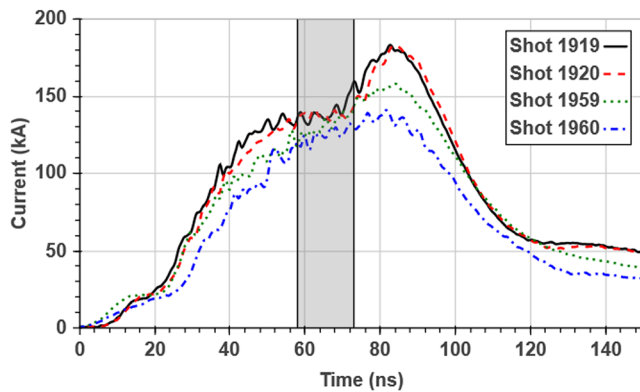


FIG. 6.  $B$ -dot measurements of the beam current using the average of four probes located behind the cathode, as shown in Fig. 1. The 15 ns spectrometer gate width is marked in gray. The current spike at the end of the pulse in shots 1919 and 1920 represents an impedance drop in the diode.

Shots 1919 and 1920 did not use the aluminum foil and were taken on a carbon-coated tantalum target and a silicon-coated tungsten target, respectively. As is typical, in shots that do not use the foil, the current is slightly higher, and the impedance collapse of the diode (signified by a rapid increase in current and a drop in voltage) is more pronounced. The C IV doublet lines shown in Fig. 5 are mostly due to contaminants in the vacuum chamber, as Shot 1919 only had about a 15% signal increase compared to Shot 1920.

The spectral fitting algorithm calculates the best-fit magnetic field by assuming a  $1/r$  decay along the line of sight, which is only true in the absence of magnetic field shielding (reduction of the magnetic field due to dense plasma formation on the anode surface and the generation of currents that oppose the azimuthal  $B$ -field produced by the electron beam) and if there is no additional current outside of the chordal position of the fiber. Without knowing the current distribution prior to this analysis, the fitting procedure represents a maximum bound on the magnetic field, as a higher magnetic field at a particular radius, due to additional current along the chordal view, can only increase the width of the spectral line shape since the Zeeman shift is proportional to the magnetic field.

Further analysis of the spectroscopic data from this diode has suggested the magnetic field is, in fact, shielded by the dense plasmas present on the anode surface.<sup>13</sup> In this case, the beam current profile cannot be determined without determining the extent of the shielding. As a result, it is not currently possible to determine an upper bound on the current density distribution from the magnetic field. The effect of  $B$ -field shielding may be studied by performing measurements at different axial distances from the anode surface, based on the expectation that the shielding effect of the anode-plasma decreases with distance from the anode. This was partially done in Ref. 13.

In the case of Fig. 5, if the assumption of no shielding were made then an enclosed current of  $83.3 \text{ kA} \pm 8.4 \text{ kA}$  would result from the measurement at  $-3.1 \text{ mm}$ . This is much less than the  $B$ -dot measurements in Fig. 6. By contrast, if the same assumption were used for the spectroscopic measurement at  $7.9 \text{ mm}$ , a current of  $158.7 \text{ kA} \pm 1.4 \text{ kA}$  would be obtained. This agrees with the  $B$ -dots, suggesting that the shielding does

not occur at this further radius. This can occur if the plasma is colder and therefore more resistive at these radii.

Uncertainties tend to increase close to the axis for several reasons. At large radii, the line of sight is essentially parallel to the magnetic field, with the  $\sigma$  component dominating the spectrum. Additionally, the spectral line shape at radii less than about  $5 \text{ mm}$  requires a high-density Stark width component, shown in Fig. 5(a) in order to reproduce the shape, resulting in higher fitting uncertainties. This is likely due to higher density plasma closer to the anode surface near the beam axis that is superimposed on lower density plasma axially off the surface. Measurements using a double-row fiber array, in which one row is placed  $0\text{-}0.5 \text{ mm}$  from the target surface, and the other row is placed  $0.5\text{-}1 \text{ mm}$  from the surface, confirm this assumption.<sup>12</sup>

The electron density is calculated from the Lorentzian components of the fits, using the upper bound of the current profiles. With Stark widths calculated at the Weizmann Institute,<sup>14</sup> Stark broadening of the C IV doublet suggests electron densities in the mid  $10^{17} \text{ cm}^{-3}$  at a  $3 \text{ mm}$  radius. This is plotted in Fig. 7. Within about  $1\text{-}2 \text{ mm}$ , the optical spectrum becomes continuum dominated with densities expected to be on the order of  $10^{19} \text{ cm}^{-3}$ . Because the Stark width continues to increase toward the beam axis, it is unlikely that these measurements are all taken from annular emission of C IV along the chordal measurement. In that case, several of the inner fibers should have similar line shapes, as they would measure C IV at similar radii.

An additional technique to confirm this assumption is to use a dopant placed in a thin strip along the diameter of the anode surface. Using line emission from this dopant, the spectral measurements can be localized. Additionally, the magnetic field can be assumed to be parallel to the line of sight, and only the outer  $\sigma$  lines would be visible.

These spectral measurements can be compared to current estimates from the  $B$ -dots. By forcing the enclosed current for the smallest radii Zeeman splitting measurement (Shot 1920 at  $3 \text{ mm}$ ) to match the  $B$ -dot estimates in Fig. 5(a) and varying only the Stark width, we obtain Fig. 8. In this case, the resulting magnetic field is too large to reflect the spectral line shape.

This analysis assumes an azimuthal magnetic field produced by the axial electron beam. However, if the magnetic

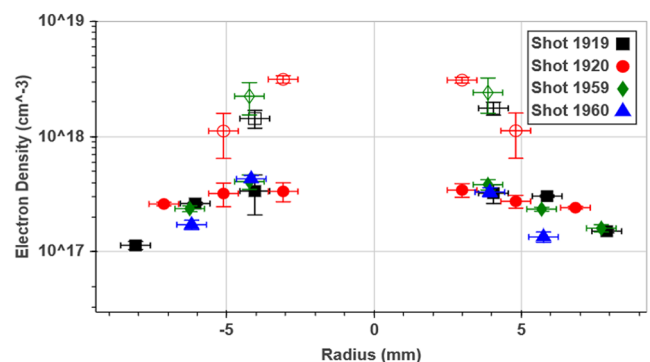


FIG. 7. Electron densities are estimated from the Lorentzian component of the C IV line fits. The line shapes are fit with an additional broader component for regions below about  $5 \text{ mm}$ , to account for a higher density (represented by hollow markers) surface in this region.

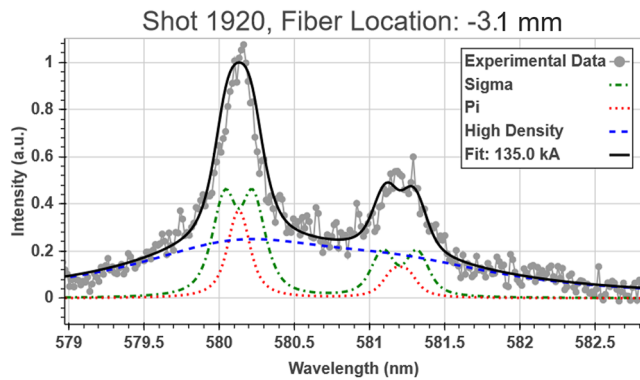


FIG. 8. Fit to the spectral line shape in Fig. 5(a), assuming the B-dot measurements of the current are within the 3 mm radius of this fiber position. The best fit, varying only the Stark width of a high and low density component, does not reproduce the line shape.

field contains an additional component that is normal to the line of sight, such as an axial component due to the presence of azimuthal currents, then this analysis would result in measurements that are too low because of higher intensity  $\pi$  line contributions along the line of sight. Additionally, if there are alternative current paths due to dense plasma formation on the surface, the x-ray spot size measurements would effectively be decoupled from magnetic field measurements. For instance, in Ref. 5 hybrid PIC/fluid simulations using the Large Scale Plasma (LSP) code suggest that the electron beam produces an annular anode plasma that extends several millimeters from the beam axis.

#### IV. CONCLUSION

In summary, we have shown a method for determining a maximum bound on the magnetic field distribution within a high power diode. The analysis suggests B-fields that range from about 4 eV at a radius of 8 mm to 5.5 T at about 3 mm from the beam axis. The method has also resulted in estimates of the electron density from the Stark broadened line profiles. Electron densities range from approximately  $10^{17}$   $\text{cm}^{-3}$  to mid  $10^{18}$   $\text{cm}^{-3}$ , depending on the axial distance from the anode surface, as shown in Fig. 7. This method does not include the effects of magnetic field shielding, which can be substantial, based on the resistivity of the particular plasma in question.<sup>13</sup>

Further improvements can also be made to these measurements. For instance, the use of dopants on the anode would isolate the location of these measurements. If the signal to noise ratios can be improved, linear polarizers may be used to separate the sigma components. Finally, independent density measurements using, for instance, interferometry would reduce fitting errors in the enclosed current estimates. These types of localized measurements may also be extended to

other applications in which the magnetic field geometry is well defined.

In conclusion, we have presented visible spectroscopic measurements within the SMP diode. These measurements demonstrate that the Zeeman spectroscopy technique can be further developed in order to obtain information on the B-field shielding effect and on the current density distribution in relativistic electron diodes.

#### ACKNOWLEDGMENTS

We would like to thank the entire RITS-6 crew for their help in fielding these experiments. Part of this work was done for the completion of a Ph.D. thesis, and so we would also like to especially thank Professors Y. Y. Lau and L. Willingale at the University of Michigan for their insights on the committee. Sandia National Laboratories is a multimission laboratory managed and operated by National Technology & Engineering Solutions of Sandia, LLC, a wholly owned subsidiary of Honeywell International, Inc., for the U.S. Department of Energy's National Nuclear Security Administration under Contract No. DE-NA0003525.

- <sup>1</sup>K. D. Hahn, N. Bruner, M. D. Johnston, B. V. Oliver, T. J. Webb, D. R. Welch, S. R. Cordova, I. Crotch, R. E. Gignac, J. J. Leckbee, I. Molina, S. Portillo, J. R. Threadgold, and D. Ziska, *IEEE Trans. Plasma Sci.* **38**, 2652 (2010).
- <sup>2</sup>N. Bennett, D. R. Welch, T. J. Webb, M. G. Mazarakis, M. L. Kiefer, M. D. Crain, D. W. Droemer, R. E. Gignac, M. D. Johnston, J. J. Leckbee, I. Molina, D. Nielsen, R. Obregon, T. Romero, S. Simpson, C. C. Smith, F. L. Wilkins, and D. Ziska, *Phys. Plasmas* **22**, 033113 (2015).
- <sup>3</sup>B. Oliver, K. Hahn, M. Johnston, and S. Portillo, *Acta Phys. Pol., A* **115**, 1044 (2009).
- <sup>4</sup>J. McCarrick, G. Caporaso, F. Chambers, Y. J. Chen, S. Falabella, F. Goldin, G. Guethlein, D. Ho, R. Richardson, and J. Weir, in *Proceedings of the 2003 Particle Accelerator Conference* (IEEE, 2003), Vol. 1, pp. 563–567.
- <sup>5</sup>N. Bruner, D. R. Welch, K. D. Hahn, and B. V. Oliver, *Phys. Rev. Spec. Top.-Accel. Beams* **14**, 024401 (2011).
- <sup>6</sup>D. R. Welch, D. V. Rose, N. Bruner, R. E. Clark, B. V. Oliver, K. D. Hahn, and M. D. Johnston, *Phys. Plasmas* **16**, 123102 (2009).
- <sup>7</sup>M. G. Mazarakis, N. Bennett, M. E. Cuneo, S. D. Fournier, M. D. Johnston, M. L. Kiefer, J. J. Leckbee, D. S. Nielsen, B. V. Oliver, M. E. Sceiford, S. C. Simpson, T. J. Renk, C. L. Ruiz, T. J. Webb, D. Ziska, D. W. Droemer, R. E. Gignac, R. J. Obregon, F. L. Wilkins, and D. R. Welch, *Phys. Plasmas* **25**, 043508 (2018).
- <sup>8</sup>E. U. Condon and G. H. Shortley, *The Theory of Atomic Spectra* (Cambridge University Press, 1951).
- <sup>9</sup>T. E. Oliphant, *Comput. Sci. Eng.* **9**, 10 (2007).
- <sup>10</sup>S. Tessarin, D. Mikitchuk, R. Doron, E. Stambulchik, E. Kroupp, Y. Maron, D. A. Hammer, V. L. Jacobs, J. F. Seely, B. V. Oliver, and A. Fisher, *Phys. Plasmas* **18**, 093301 (2011).
- <sup>11</sup>Prism Computational Sciences, Inc., PrismSPECT, 1998.
- <sup>12</sup>S. G. Patel, Ph.D. thesis, University of Michigan, Ann Arbor, 2016.
- <sup>13</sup>S. Biswas, R. Doron, D. Mikitchuk, and Y. Maron, M. D. Johnston, S. G. Patel, M. L. Kiefer, and M. E. Cuneo, "Shielding of the azimuthal magnetic field by the anode plasma in a relativistic self-magnetic-pinch diode," *Phys. Plasmas* (submitted).
- <sup>14</sup>E. Stambulchik and Y. Maron, *J. Quant. Spectrosc. Radiat. Transfer* **99**, 730 (2006).